EGTRIB Journal

JOURNAL OF
THE EGYPTIAN SOCIETY OF TRIBOLOGY
VOLUME 20, No. 4, October 2023, pp. 88 - 105 **ISSN 2090 - 5882**

(Received June 09. 2023, Accepted in final form September 08. 2023) **jest.journals.ekb.eg**

IMPACT OF TOOL WEAR ON THE UTMOST TEMPERATURE DURING THE FRICTION STIR WELDING

Hewidy A. M. and Sabry I.

Department of Mechanical Engineering, Faculty of Engineering, Benha University, Benha, 13511, Egypt.

ABSTRACT

Friction stir welding (FSW) is a solid-state welding method that involves joining two workpieces by applying pressure and significant plastic deformation close to their melting temperatures. The impact of rotation speed, travel speed, axial force, maximum temperature, and tool wear in the friction stir welding (FSW) process is significant. The present study examines the impact of three specified variables on the maximum temperature, ultimate tensile strength (UTS), and tool wear of friction stir welding (FSW) of 6063-T6 and 6060-T6 alloys. Response Surface Methodology (RSM) has been employed as an auxiliary method. The total amount of material removed from the tool wear was found to be directly proportional to the rotational speed but inversely proportional to the travel speed and axial force. The increase in rotation speed leads to higher tool wear but reduces the surface roughness of the tool. The findings indicate that the parameter with the most significant impact on the maximum attained temperature is 1800 rpm rotation speed and 4 mm/min travel speed, I KN axial force.

KEYWORDS

Friction stir welding, dissimilar aluminum, rotation speed, tool wear, temperature, ultimate tensile strength.

INTRODUCTION

Friction stir welding (FSW) is a solid-state welding method in which two workpieces are joined by applying pressure and significant plastic deformation close to their respective melting points, [1]. Compared to alternative procedures, Friction Stir Welding (FSW) offers several advantages, such as reduced energy requirements, decreased residual stress levels, improved mechanical qualities, fewer flaws, and environmentally friendly characteristics, [2]. This procedure is employed to combine elements that are both similar and distinct. Heat generation and adequate distribution are the primary determinants in establishing suitable and flawless bonding in the Friction Stir Welding (FSW) process. The generation of heat in friction stir welding (FSW) is attributed to the combined effects of friction and plastic deformation, [3]. According to Mishra et al., [4], the primary source of heat

generation in machining processes is the frictional interaction between the tool and the workpiece. The formation of distinct zones in workpieces is attributed to the unequal heat distribution in FSW. The observed dissimilarities between these locations can be attributed to plastic deformations, heat distributions, residual stresses, and microstructure variations. In FSW using dissimilar materials, the precise management of heat distribution is of utmost significance. They are primarily owing to the mechanical and thermal properties exhibited by the materials involved, resulting in a pronounced asymmetry in heat distribution at the joints. In order to mitigate this drawback, it is necessary to offset the tool from the weld line, [5]. According to Essa et al., [6], using the offsetting Pin from the shoulder is a novel approach for achieving uniform heat distribution in workpieces. Displacing the pin results in an augmentation of the flow of plastic material inside a fixed pin volume, hence resulting in an expansion of the area of the welded cross-section.

Numerous studies have been conducted on the topic of tool offsetting. The study conducted by Ramachandran et al., [7], examined the impact of tool offset distance on the mechanical characteristics and microstructures of HSLA steel (as the retreating side) and AA5052-H32 aluminum alloy during friction stir welding. The findings indicate that the offset distance can significantly influence the mechanical characteristics and microstructures. In their study, Khan et al., [8], examined the impact of tool offset distance and shoulder penetration on defects occurring in the friction stir welding (FSW) process of AA5083-H116 (as the advancing side) and AA6063-T6. It was discovered that shifting towards the more ductile side effectively prevents tunnel flaws and results in a notable increase in ultimate tensile strength (UTS). In their study, Shah et al. [9] examined the impact of tool eccentricity on the material flow during the friction stir welding (FSW) process of AA6061. Their findings indicated that the introduction of offsetting resulted in an augmentation of both the material flow and the weld area.

The study conducted by Naghibi et al., [10], examined the impact of tool offsets on the UTS of weld joints made from AA5052 and AISI 304. The researchers also employed a genetic algorithm to optimize the UTS. The study by Liang et al., [11], examined the impact of process parameters and tool offset on the mechanical properties of the weld junction between aluminum and magnesium alloys, explicitly focusing on the advancing side. Concerning their research, it has been observed that in various rotational speeds, the introduction of offsetting towards either aluminum or magnesium alloy results in a decrease in ultimate tensile strength (UTS). It was aimed to examine the influential factors involved in friction stir welding (FSW) of two dissimilar metals, copper and aluminum.

The study by R. Srinivasan et al., [12], examined the impact of offsetting on the flow of materials during friction stir welding (FSW) of aluminum and titanium. The research revealed that the process of axial forces causes a significant rise in the flow of materials. In this study, Sabry et al., [13], investigated the impact of process parameters and rotation speed and travel speed on the occurrence of defects during friction stir welding (FSW) of 6061. The findings of the study indicate that the tool offset has a significant impact on the mechanical properties of the weld. In their study, Marathe Shalin et al. [14] optimized the mechanical properties of a joint formed using

friction stir welding (FSW) of AA6061. This was achieved by examining the impact of tool rotation speed and tool pin profile.

In their study, P. Sevvel et al., [15], examined the impact of axial force and tool geometry on the mechanical properties of AZ80A Mg alloy in an advancing side weld joint. Their research aimed to determine the optimal value of axial force.
Sabry et al., [16], investigated the impact of rotation speed, clamping torque, and clamping pith on the mechanical parameters of the weld joint between AA6061, explicitly focusing on the advancing side. It was discovered that the maximum ultimate tensile strength (UTS) is attained when there is 30 mm, 1800 rpm, and 70 Nm for the take-into-consideration parameter range for the Clamp Pitch, rotational speed, and Clamping Torque, respectively.

Rethmeier M. et al., [17], examined the effects of four distinct traverse forces, axial force, and tool torque on the friction stir welding (FSW) process of AA2024-T4. The researchers identified the optimal offset that resulted in an increase in the weld area and improvements in the microstructure and mechanical properties of the welded material.

The study conducted by Mouminah Amatullah et al., [18], examined the impact of rotational speed on the mechanical and microstructural properties of the various aluminum alloys. The influence of process parameters, including tool rotational speed, tool traverse speed, and tool shape, is crucial for achieving welds without defects and enhancing joint efficiency.

Furthermore, the material location influences the joint's mechanical qualities, temperature distribution, and plastic flow in addition to the parameters of tool offset and pin offset previously described, [19]. The function of the material position is significant in determining a joint's temperature distribution, mechanical characteristics, and microstructureowing to the asymmetry of plastic flow on either side of the welding line, [20]. Numerous studies have been conducted on friction stir welding (FSW) of dissimilar metals; nevertheless, the influence of material position on temperature distribution and maximum temperature has received limited attention. This study investigates the concurrent impact of rotation speed, travel speed, and axial force on process temperature in dissimilar friction stir welding (FSW) of 6063-T6 and 6060-T6 aluminum alloys. The experimental approaches are employed, which have not been previously employed. In order to examine the impact of the three variables mentioned above on the maximum temperature, UTS, and tool wear rate in the process, the research employed Response Surface Methodology (RSM).

Materials and Methods

Materials

In the present investigation, two distinct aluminum alloys, 6063-T6 and 6060-T6, were employed to conduct the FSW procedure.

Table 1. The weight percentages of the chemical composition of two aluminum alloys, namely 6063-T6 and 6060-T6.

Weight (%)	Al	Si	Fe	Cu	Mn	Mg	Cr	Zn	Ti
6063-T6	Balance	0.2	0.3	0.1	0.1	0.9	0.01	0.1	0.12
6060-T6		0.6	0.3	0.7	0.15	0.8	0.35	0.25	0.15

Table 2. Mechanical characteristics of 6063-T6 and 6060-T6.

	Ultimate Tensile Strength	Elongation (%)	Vickers Hardness
6063	240	12	85
6060-T6	215	12	75

Table 3. Mechanical characteristics of SS316.

	Ultimate Tensile Strength	Yield Strength (MPa)	Vickers Hardness
SS316	480	175	95

This method created two workpieces measuring 100 × 70 × 6 mm^3 for welding. A tool made of SS316L was utilized for FSW. The mechanical properties of SS316L are given in Table 3.

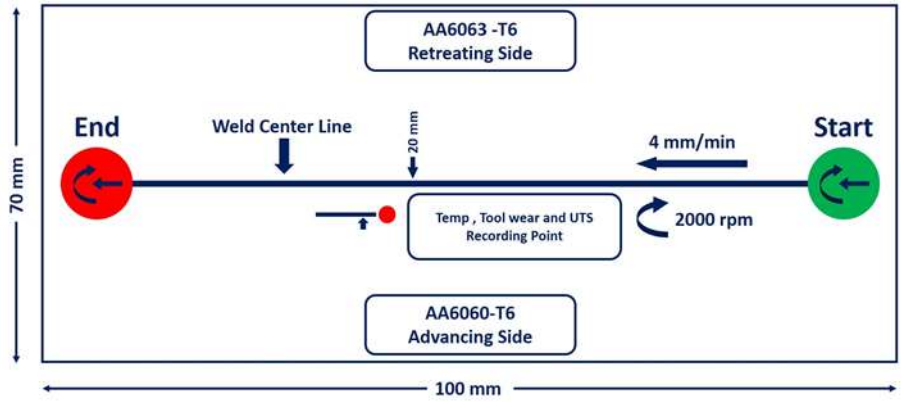

Fig. 1 The process flow diagram for FSW.

The geometric dimensions are depicted in Fig. 2. The conical Pin was specifically engineered to facilitate the seamless insertion of the tool into the specimen during the penetration procedure. Consequently, the FSW tool was fabricated based on the geometric measurements outlined in Table 4.

Table 4. Geometric dimensions of the FSW tool refer to the physical characteristics.

length of tool	**59**
diameter of Pin (tip)	**0.9 mm**
length of Pin	**2.9mm**
diameter of Pin (shoulder or near)	**1.9 mm**
diameter of Shoulder	**20 mm**
angle of tilt	**2.25**

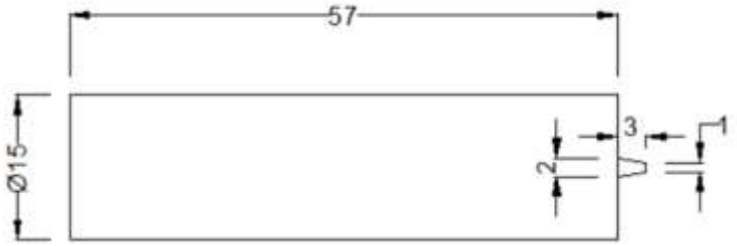

Fig. 2 The tool's geometric measurements (all measurements are in mm).

The FSW technique was conducted utilizing a milling machine, and a suitable fixture was produced before investigating five cases. In order to measure the temperature of welded specimens, an infra-red thermometer was affixed to the mobile component of the milling machine, ensuring that it moved at the same pace as the FSW speed of travel. The temperature history of a location at a distance of 15 mm from the weld line on the advancing side was recorded during each FSW procedure, as depicted in Fig. 1. Figure 3 displays the weld apparatus and thermometer. Furthermore, Figure 4(a) depicts welded specimens utilizing five distinct techniques.

Fig. 3. FSW set-up.

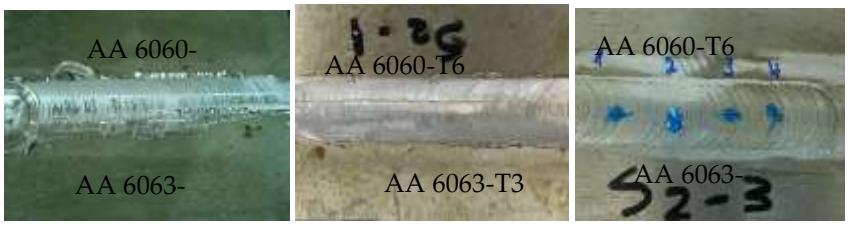

Fig. 4 (a) Specimens welded using various tools.

Tensile test

Three tensile specimens were manufactured for each experiment following the ASTM E8M-04 standard. The ultimate tensile strength (UTS) of the friction stir welding (FSW) joints was evaluated using universal testing equipment. The obtained data, consisting of three measurements, has been summarized in Figure 4 (b), showcasing the average values.

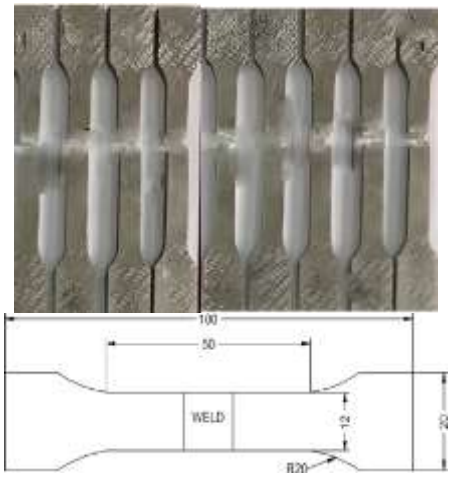

Fig. 4 (b) The tensile test specimen.

Temperature

Two type-K thermocouples were employed to ascertain the temperature at positions situated 3 mm from the weld line along the lateral axis of the specimen. The objects mentioned above were carefully placed within pre-drilled cavities measuring 1 mm in diameter and 1 mm in depth, located on the lower surface of the flange component. Figure 4 (c) displays a schematic illustration depicting the spatial arrangement of the thermocouples. Statistical analysis was conducted using the average temperature value. The specimen used for tensile testing is characterized by its dimensions, expressed in millimeters.

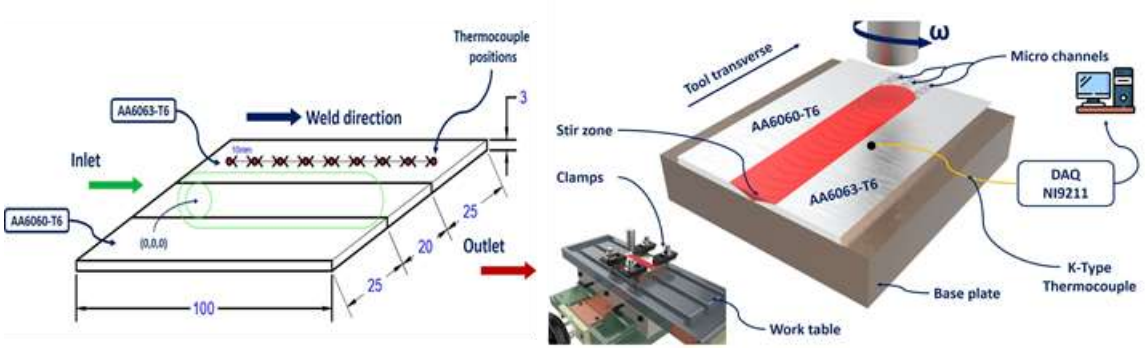

Fig. 4 (c) The position of the thermocouple.

Tool wear

The evaluation of the wear resistance performance of a tool can be conducted by measuring the extent of mass and volume loss experienced by the tool. In this study, the wear evaluation is conducted by quantifying the weight reduction of each tool steel after FSW. In this study, tool wear is measured by quantifying the weight reduction of the tool steels subsequent to the FSW process applied to AA6060-T6 and AA6063-T6 plates. The weight of the tool steel specimen is determined prior to performing FSW using a precision scale capable of measuring up to three decimal places in the unit of grams (g). The tool's weight is afterward measured using the identical balance following the execution of FSW. The spindle speed for FSW is configured at three levels: 1000, 1400, and 1800 rpm. The tool travel speed is set at 4.8 and 10 mm/min, while the axial force is applied at 1, 1.5, and 2 KN., shown as the schematic representation tool wear Fig. 4 (d). These parameter settings are chosen to ensure sufficient heat generation for material plasticization and to minimize the probability of tool failure. The weight loss and percentage wear for each tool SS316L are presented and seen in Table 6. The calculation of the percentage wear is determined by the utilization of Equation 1, wherein mi represents the original mass of the tool SS316L, and Δm signifies the tool's mass alteration

$$\frac{\Delta m}{m_i} \times 100 \quad Eq.1$$

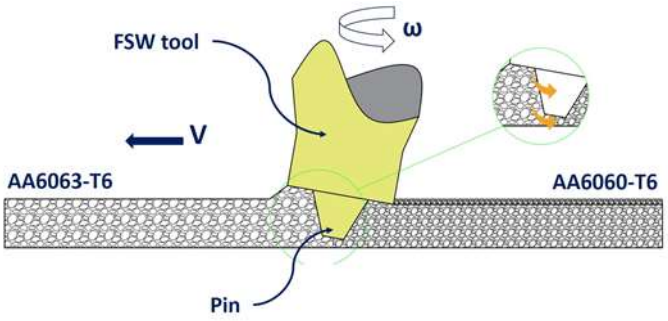

Fig. 4 (d) Schematic representation tool wear.

Design of experiments (DOE)

Following the validation of the numerical model, this study proceeds to elucidate the design of the experiments employed. The present study examined three variables: speed of rotation, speed of travel, axial forces as quantitative inputs, and the position of alloys as qualitative inputs. The outputs of interest were the maximum temperature, UTS, and wear rate during the operation. It is worth noting that the highest temperature in the FSW process was attained near the weld line and the bottom of the tool shoulder. The temperature can be measured using thermocouples. The Central Composite Design (CCD) examined the primary effects and interactions. The MINITAB program employed this strategy and analyzed variance (ANOVA), [21]. The study examined each quantitative variable at five distinct levels, whereas the qualitative variable was supposed to have two levels. Table 5 presents a depiction of the input variables and their corresponding levels.

Table 5. Levels of the input variables.

Process Parameters	Unit	Symbol	Levels		
			-1	0	1
speed of rotation	RPM	N	1000	1400	1800
speed of travel	mm/min	S	4	8	10
Axial force	KN	F	1	1.5	2

Table 6. Design matrix and output parameters.

Run	FSW process parameters			Responses		
	N	S	F	Temperature	UTS	Tool wear
1	1800	10	2.0	625.81	195.460	0.918743
2	1400	10	2.0	581.64	185.414	0.800432
3	1000	10	2.0	537.47	175.369	0.787898
4	1800	8	2.0	640.77	198.328	0.987977
5	1400	8	2.0	596.60	188.282	0.895980
6	1000	8	2.0	552.43	178.237	0.745950
7	1800	4	2.0	670.69	204.064	0.818743
8	1400	4	2.0	626.52	194.018	0.700432
9	1000	4	2.0	582.36	183.973	0.687898
10	1800	10	1.5	622.85	191.495	0.287977
11	1400	10	1.5	578.68	181.449	0.225980
12	1000	10	1.5	534.51	171.404	0.205950
13	1800	8	1.5	637.81	194.363	0.618743
14	1400	8	1.5	593.64	184.318	0.564320
15	1000	8	1.5	549.47	174.272	0.587898
16	1800	4	1.5	667.74	200.099	0.587977
17	1400	4	1.5	623.57	190.054	0.425980
18	1000	4	1.5	579.40	180.008	0.412595
19	1800	10	1.5	619.89	187.530	0.405950
20	1400	10	1.0	575.73	177.485	0.418743
21	1000	10	1.0	531.56	167.439	0.364320
22	1800	8	1.0	634.86	190.398	0.387898
23	1400	8	1.0	590.69	180.353	0.387977
24	1000	8	1.0	546.52	170.307	0.225980
25	1800	4	1.0	667.74	200.099	0.212595
26	1400	4	1.0	620.61	186.089	0.205950
27	1000	4	1.0	576.44	176.044	0.135950

RESULTS AND DISCUSSION

Outcome of experimental

In order to examine the impact of primary components and their interactions on the maximum temperature of a given process, a Central Composite Design (CCD) methodology was employed, [22]. A second-order polynomial was utilized to model

the maximum temperature. A design matrix was created, and its details are presented in Table 6. Furthermore, Table 6 presents the depicted output variables, precisely the maximum temperatures.

In the context of statistical investigations, the metrics of R-squared and adjusted R-squared are utilized to assess the precision of a polynomial model. A higher proximity to unity for these parameters indicates greater accuracy. The statistical values of the parameters have been presented in Table 8.

The reliability factor was selected at a confidence level of 95 %. The analysis of variance (ANOVA) method was employed, and the results are presented in Table 8. The efficacy of each variable was assessed based on its P value, which should be less than 5%, to ensure a dependability level of 95 %. The coefficients were selected based on the P values presented in Table 8. To validate the fitted model, several checks were performed, including assessing the normality of the data, examining the stability of variances across different levels, and evaluating the independence of the data across time.

Table 7. Coefficients of the statistical model.

	UTS				
Source	**Sequential p-value**	**Lack of Fit P-value**	**Adjusted R^2**	**Predicted R^2**	
Linear	**< 0.0001**	**0.9931**	**0.9879**	**0.9842**	**Suggested**
2FI	**0.0766**	**0.9980**	**0.9900**	**0.9831**	
Quadratic	**0.6829**	**0.9972**	**0.9892**	**0.9807**	
Cubic	**0.5294**	**0.9991**	**0.9889**	**0.9749**	**Aliased**
	Temperature				
Linear	**< 0.0001**	**0.9931**	**0.9996**	**0.9995**	**Suggested**
2FI	**0.0772**	**0.9980**	**0.9997**	**0.9995**	
Quadratic	**0.6795**	**0.9972**	**0.9997**	**0.9994**	
Cubic	**0.5273**	**0.9991**	**0.9996**	**0.9992**	**Aliased**
	Wear rate				
Linear	**< 0.0001**	**0.4442**	**0.7040**	**0.6547**	
2FI	**0.7790**	**0.4255**	**0.6773**	**0.6026**	
Quadratic	**0.0093**	**0.5269**	**0.8036**	**0.6805**	**Suggested**
Cubic	**0.1511**	**0.5970**	**0.8617**	**0.6579**	**Aliased**

Table 8. Considered model's ANOVA.

UTS						
Source	**Sum of Squares**	**df**	**Mean Square**	**F-value**	**p-value**	
Model	**2528.16**	**9**	**280.91**	**266.28**	**< 0.0001**	**Significant**

A-Rotation speed	**1022.37**	**1**	**1022.37**	**969.14**	**< 0.0001**	
B-Travel speed	**372.94**	**1**	**372.94**	**353.52**	**< 0.0001**	
C-Axial force	**191.34**	**1**	**191.34**	**181.37**	**< 0.0001**	
AB	**4.24**	**1**	**4.24**	**4.02**	**0.0611**	
AC	**0.8387**	**1**	**0.8387**	**0.7950**	**0.3850**	
BC	**1.74**	**1**	**1.74**	**1.65**	**0.2162**	
A^2	**0.0070**	**1**	**0.0070**	**0.0067**	**0.9358**	
B^2	**0.0581**	**1**	**0.0581**	**0.0551**	**0.8172**	
C^2	**1.48**	**1**	**1.48**	**1.41**	**0.2518**	
Residual	**17.93**	**17**	**1.05**			
Lack of Fit	**10.07**	**16**	**0.6296**	**0.0801**	**0.9972**	**Significant**
Pure Error	**7.86**	**1**	**7.86**			
Cor Total	**2546.09**	**26**				
Temperature						
Model	**45065.43**	**9**	**5007.27**	**8514.58**	**< 0.0001**	**Significant**
A-Rotation speed	**19388.30**	**1**	**19388.30**	**32968.72**	**< 0.0001**	
B-Travel speed	**8260.19**	**1**	**8260.19**	**14045.99**	**< 0.0001**	
C-Axial force	**106.29**	**1**	**106.29**	**180.74**	**< 0.0001**	
AB	**2.36**	**1**	**2.36**	**4.01**	**0.0616**	
AC	**0.4715**	**1**	**0.4715**	**0.8017**	**0.3831**	
BC	**0.9637**	**1**	**0.9637**	**1.64**	**0.2177**	
A^2	**0.0041**	**1**	**0.0041**	**0.0069**	**0.9347**	
B^2	**0.0312**	**1**	**0.0312**	**0.0530**	**0.8206**	
C^2	**0.8385**	**1**	**0.8385**	**1.43**	**0.2489**	
Residual	**10.00**	**17**	**0.5881**			
Lack of Fit	**5.62**	**16**	**0.3510**	**0.0801**	**0.9972**	**Significant**
Pure Error	**4.38**	**1**	**4.38**			
Cor Total	**45075.43**	**26**				
Tool wear rate						
Model	**1.45**	**9**	**0.1608**	**12.82**	**< 0.0001**	**Significant**
A-Rotation speed	**0.0266**	**1**	**0.0266**	**2.12**	**0.1632**	
B-Travel speed	**0.0000**	**1**	**0.0000**	**0.0021**	**0.9643**	
C-Axial force	**1.06**	**1**	**1.06**	**84.57**	**< 0.0001**	
AB	**0.0047**	**1**	**0.0047**	**0.3771**	**0.5473**	

AC	**0.0097**	**1**	**0.0097**	**0.7750**	**0.3910**	
BC	**0.0022**	**1**	**0.0022**	**0.1790**	**0.6775**	
A^2	**0.0000**	**1**	**0.0000**	**0.0015**	**0.9693**	
B^2	**0.0964**	**1**	**0.0964**	**7.68**	**0.0131**	
C^2	**0.0856**	**1**	**0.0856**	**6.83**	**0.0182**	
Residual	**0.2132**	**17**	**0.0125**			
Lack of Fit	**0.2062**	**16**	**0.0129**	**1.85**	**0.5269**	**Significant**
Pure Error	**0.0070**	**1**	**0.0070**			
Cor Total	**1.66**	**26**				

The regression equations for maximum temperature, UTS, and tool wear rate in FSW as a function of the factors under consideration are presented in Table 9.

Table 9. The final regression equations for the maximum process temperature, UTS, and minimum tool wear.

UTS	**=**	**+150.35474 +0.025143 N-1.57226 S +7.50412 F**
Temperature	**=**	**+491.23991+0.110445 N-7.58408 S +5.59401 F**
Tool wear%	**=**	**-0.463437 +0.000113 N+0.004292 S +0.522239 F**

The primary factors and their interrelationships

According to the analysis of variance (ANOVA) and the relationships presented in Table 9, it can be observed that all the variables have a direct impact on the maximum temperature, UTS, and tool wear percentage. According to the statistical analysis in Table 8, the F and P values indicate that rotation speed significantly influences the maximum temperature, UTS, and tool wear. Specifically, rotation speed significantly impacts maximum temperature, followed by axial force, and has the most minor effect on tool wear. Figure 5 illustrates the relationship between the maximum temperature, rotation speed, travel speed, and axial forces.

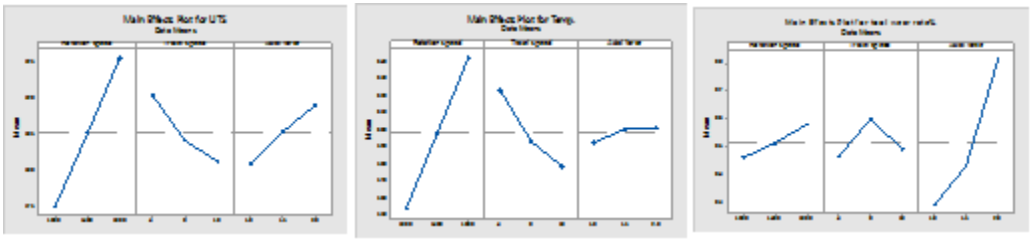

Fig. 5. Main effects plot of rotation speed, travel speed, and axial force UTS (b) temperature (C), and (c) tool wear percentage.

The data analysis in Fig. 5 (a) indicates a significant decrease in the maximum temperature. Furthermore, it is observed that this decline becomes more pronounced as the travel speed increases. The plastic flow within a larger workpiece area is enhanced as the travel speed in the constant volume is increased. The augmentation in travel speed increases plastic flow while simultaneously causing a decrease in plastic flow concentration at the middle region of the welded cross-section. As a result of this drop in concentration, the heat generated by friction and plastic flow is

dispersed across a larger surface area, reducing the workpiece's maximum temperature. A study by Mourad et al., [23], yielded a comparable outcome.

According to the data presented in Fig. 5 (b), it can be observed that increasing the travel speed towards either the advancing or retreating side reduces the maximum temperature. Furthermore, this reduction is more pronounced when the tool rotation speed is directed towards the advancing side. Tool rotation speed generates non-homogeneous and non-uniform flow due to an imbalance in plastic flow, leading to a subsequent decrease in the maximum temperature. Lower plastic flow is observed on the advancing side due to the opposing rotational speed and traveling speed of the counter money, in contrast to the retreating side. Hence, as the tool's travel speed increases towards the advancing side, there is a more pronounced decrease in plastic flow. Consequently, this reduction in material flow leads to a more significant decrease in the maximum temperature.

The effects of rotation speed travel speed have been extensively investigated by researchers, revealing significant alterations in heat distribution, plastic flow behavior, and joint qualities. According to the findings of Mourad et al., [24], it has been observed that the increased rotation speed and decreased travel speed duo increase the mechanical properties of the joint. A. Balamurugan et al., [25] have demonstrated instances when the opposite is true. According to the findings derived from Fig. 9, the maximum temperature exhibits a more significant increase in 1800 rpm compared to 1000 rpm rotation speed. The plastic flow is hindered on the advancing side due to an imbalance in FSW. If a more resilient alloy is positioned on the advancing side, the transition of the material to the plastic phase will occur at a lower temperature. This is because the presence of the harder alloy reduces the plastic flow, resulting in a decrease in the maximum temperature.

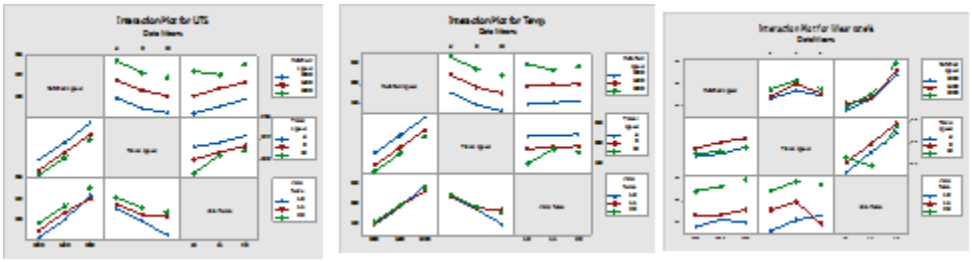

Fig. 6 Process interaction between speed of rotation, speed of travel, and axial force (a) UTS, (b) temperature (C), and (c) tool wear percentage.

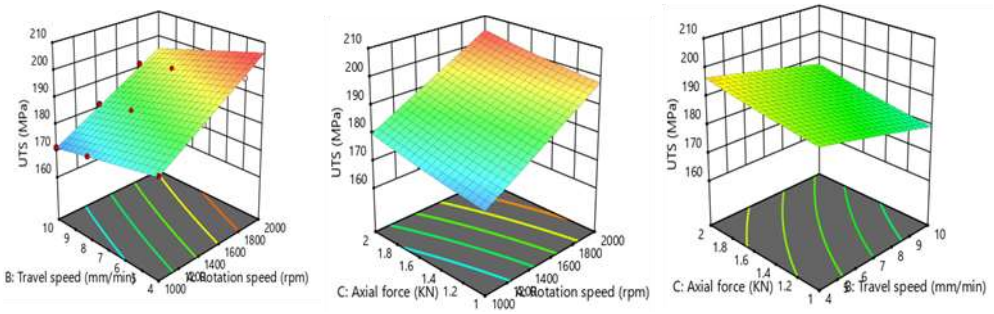

Fig. 7 Contour plots show how the axial force, weld speed, and speed of rotation affect the FSW joints UTS.

Figure 8 illustrates the interplay between rotation speed, weld travel speed, axial force, and temperature. The impact of rotation and travel speed on temperature while maintaining axial force is depicted in the 3D contour plots (Figure 8a). The impact speed of rotation and axial force on temperature while maintaining a constant weld transit speed is seen in the 3D contour plots (Fig. 8b). The impact speed of travel and axial force on temperature while maintaining a constant rotation speed is depicted in the 3D contour plots (Fig. 8c), consistent with the study by K.P. Yuvaraj et al., [26].

The plot analysis reveals that the highest temperature, reaching an optimal value of 670 degrees Celsius, is achieved when the rotation speed is set at 1800 revolutions per minute and the travel speed is maintained at 4 millimeters per minute. The temperature will tend to decline or increase when there is a deviation from the specified values of rotation speed and travel speed. Figure 8 illustrates the combined influence of axial force and rotation speed while maintaining a constant travel speed of 4 mm/min. Based on the analysis of the 3D plots, it is apparent that the optimal temperature is approximately 670 degrees Celsius when the rotation speed is set at 1800 revolutions per minute and the axial force is maintained at 1 kilonewton.

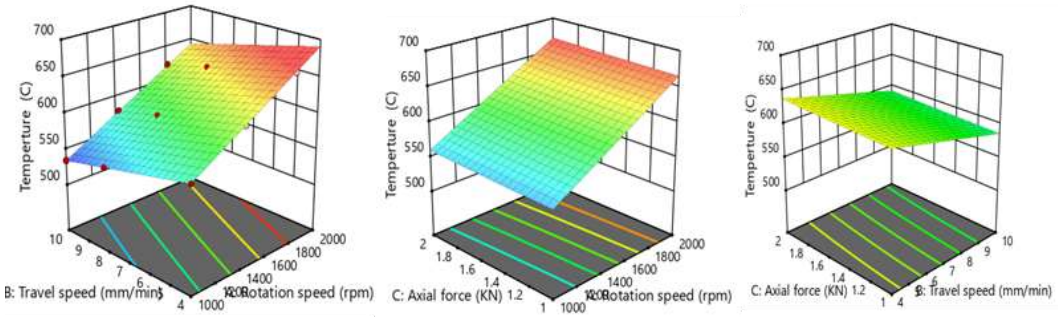

Fig. 8 Contour plots show how the axial force, weld speed, and rotation speed affect the temperature of an FSW joins.

Figure 9 illustrates the interaction effects of speed of rotation, speed of travel, and axial force on the tool wear. The effect of rotation and travel speed on tool wear while maintaining axial force is depicted in the 3D contour plots (Fig. 9 a). The impact of the speed of rotation and axial force on tool wear while maintaining a constant weld transit speed is depicted in the 3D contour plots (Figure 9 b). The impact of travel speed and axial force on tool wear while maintaining a constant rotation speed is demonstrated through 3D contour plots (see Fig. 9 c).

The analysis of the figure reveals that the optimal tool wear, amounting to 0.296%, is achieved when the rotation speed is set at 1800 rpm and the travel speed is maintained at 4 mm/min. The temperature tends to fall or increase when there are deviations from the specified speed values of rotation and travel. Figure 8 depicts the interaction impact of axial force and speed of rotation while maintaining a constant speed of travel of 4 mm/min. Based on the analysis of the 3D plots, it can be observed that the optimal level of tool wear occurs at approximately 0.818 %. This optimal condition is

achieved when the rotation speed is set at 1800 rpm and the axial force is maintained at 1 KN.

Findings from Optimization

The better welding parameters for producing the desired mechanical quality of the welded connection have been determined by optimization research, [27]. These circumstances were selected based on specific optimization criteria outlined in Table 5. Based on the experimental findings and optimization results, it is evident that achieving optimal UTS and temperature requires a rotation speed of approximately 1800 rpm. This indicates that the responses are influenced mainly by rotation speed compared to other input factors. This is consistent with the study, [28]. Figure 10 displays the contour and overlay plots, which provide predictions for the optimal UTS of 204 MPa and temperature of 688 °C. These predictions are based on the optimal welding conditions, including speed of rotation of 1800 rpm, speed of travel of 4 mm/min, and axial force of 1 KN. Figure 10 displays the contour and overlay plots, which predict the optimal tool wear of 0.286. These predictions are based on the optimal welding conditions, including a speed of rotation of 1800 rpm, speed of travel of 4 mm/min, and axial force of 1 KN.

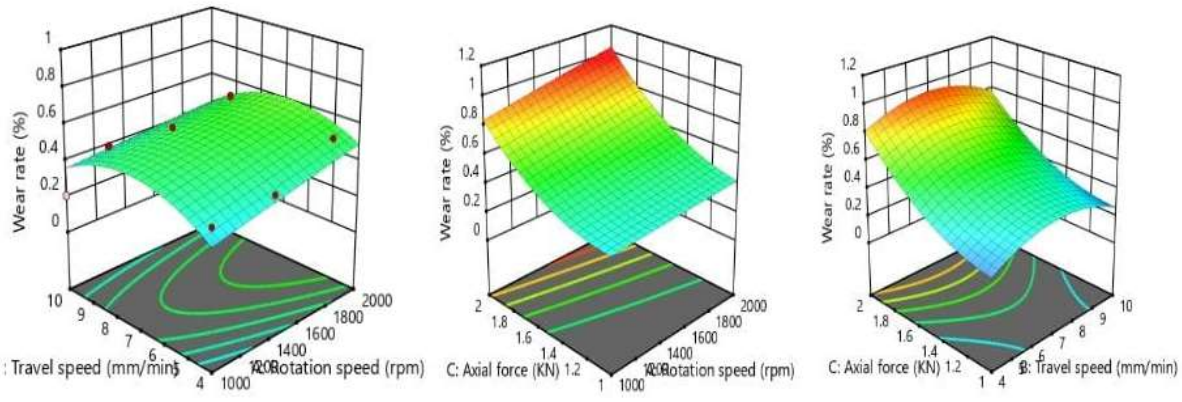

Fig. 9 Contour plots show how the axial force, weld speed, and rotation speed affect the tool wear of an FSW join.

Approval of the created model

The desirability approach model is assessed for its accuracy using experimental data. The errors for all 27 runs are determined and presented in Table 6, which includes the actual value, predicted value, and error % for the ultimate tensile strength (UTS), temperature, and tool wear. The empirical equations created by the design expert software are utilized to determine the expected values, while the actual values are obtained through the conduction of experiments. The UTS exhibits a percentage error range of -0.82 to +1.71. Likewise, the error % for temperature and tool wear falls between -1.223 to +1.14 and -0.234 to +0.156, respectively. Therefore, it is evident that the recently created model has accurately predicted UTS, temperature, and tool wear in close agreement with the experimental data.

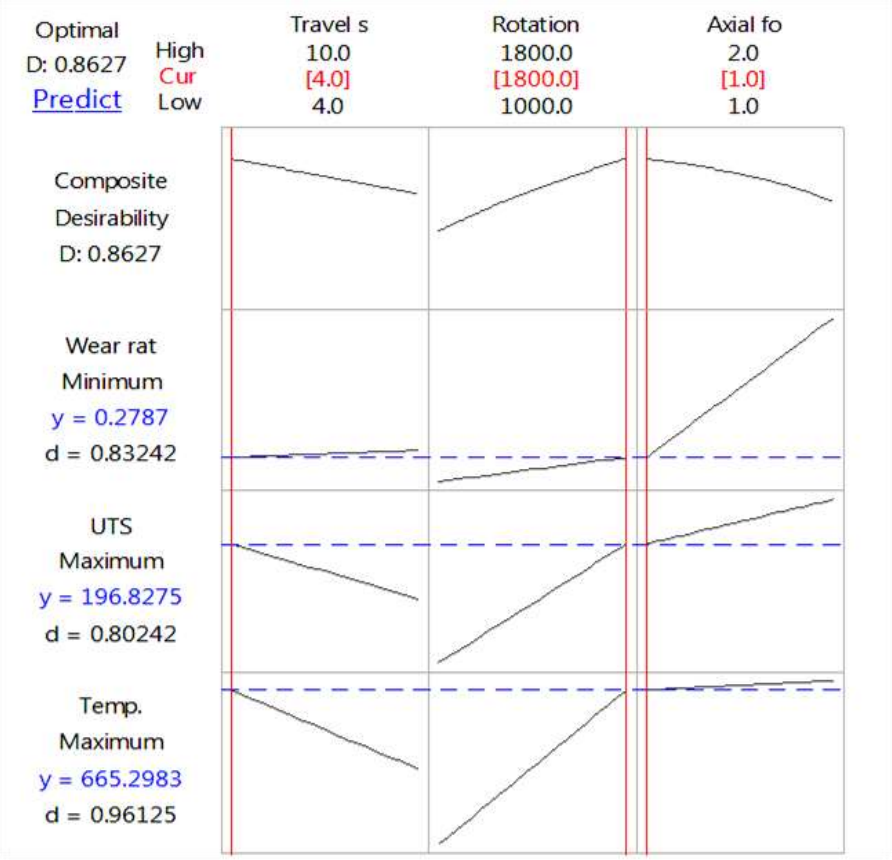

Fig. 10 A map that forecasts the ideal FSW process parameters.

The model is also verified against the expected ideal welding conditions. Three confirmation experiments were conducted using a rotation speed of 1800 revolutions per minute (rpm), a travel speed of 4 millimeters per minute (mm/min), and an axial force of 1 K N. The predicted maximum percentage errors for the optimum UTS, temperature, and tool wear are 1.027%, 0.766%, and 0.11189%, respectively.

CONCLUSIONS

This research investigates FSW's experimental and modeling aspects applied to two dissimilar alloys, AA6063-T6 and AA6060-T6. The study examines the influence of rotation speed, travel speed, and axial force on critical parameters such as the maximum process temperature, UTS, and tool wear. In order to examine the effect of the three factors mentioned above on the maximum temperature, UTS, and minimal tool wear of the process, the researchers employed the RSM. The ensuing outcomes of this investigation are as follows:

1. **The utilization of the three-factorial Box-Behnken experimental design has proven to be effective in establishing the correlation between the responses, namely UTS, temperature, and tool wear, and the input parameters, which include speed of rotation, speed of travel, and axial force. Experiments were conducted to maximize the UTS, temperature, and tool wear by selecting three levels for each parameter.**
2. **According to the analysis of variance (ANOVA), the variable that had the most significant impact on the maximum temperature and ultimate tensile strength (UTS)**

was the rotation speed. A decrease in maximum temperature was noted when travel speed decreased.

3. **The variables that impact the maximum process temperature are ranked in the following order of importance: rotational speed, speed of travel, and axial force.**
4. **In this study, perturbation plots and 3D contour plots were constructed to examine the interaction effects of welding parameters. The parameter that exerts the most influence is the speed of rotational. The optimal UTS, tool wear and temperature were determined to be 204 MPa, 0.296, and 670 °C, respectively. These values were obtained under specific welding conditions, including a rotation speed of 1800 rpm, a speed of welding 40 mm/min, and an axial force of 1 kN.**
5. **The efficacy of the desirability approach is demonstrated through the successful implementation of the Box-Behnken method in all 27 conducted trials. The experimental findings yielded optimal values of 204 MPa for UTS, 0.296 % for tool wear, and 670 °C for temperature. These values were obtained under the welding conditions of 1800 rpm rotational speed, 40 mm/min speed of travel, and an axial force of 1 kN.**

REFERENCES

1. **Balamurugan A., Bhuvaneswari M., Suresh K.C., Sudha M., "Investigation on the mechanical properties of FSWed AA6063 – T351 aluminum alloy joints", Materials Today: Proceedings, (2023), https://doi.org/10.1016/j. matpr. 2023.05.553.**
2. **Hewidy A. M., sabry I., "Underwater friction-stir welding of a stir-cast AA6061-SiC metal matrix composite: optimization of the process parameters, microstructural characterization, and mechanical properties", Materials Science-Poland, 40(1)pp. 101-115, (2022), https://doi.org/10.2478/msp-2022-0013.**
3. **Shah L. A., Sonbolestan S., Midawi A. H., Walbridge S. & Gerlich A., "Dissimilar friction stir welding of thick plate AA5052-AA6061 aluminum alloys: effects of material positioning and tool eccentricity", The International Journal of Advanced Manufacturing Technology, 105, pp.889–904, (2019), https://doi.org/10. 1007/s00170-019-04287-9.**
4. **El-Kassas A. M., Sabry I., Mourad A-H. I., Thekkuden D. T., "Characteristics of Potential Sources - Vertical Force, Torque and Curent on Pénétration depth for Quality Assessment in Friction Stir Welding of AA 6061 Pipes", International Review of Aerospace Engineering, 12(4), pp. 195-207, (2019), DOI: 10.15866/irease. v12i4. 16362.**
5. **Essa A. S., Ahmed M. Z. , El-Nikhaily A. E., "An analytical model of heat generation for eccentric cylindrical pin in friction stir welding", Journal of Materials Research and technology, 5(3), pp. 234-240, (2016), https://doi.org/10.1016/j. jmrt. 2015.11.009.**
6. **Naghibi H. D., Shakeri M., Hosseinzadeh M.,"Neural network and genetic algorithm based modeling and optimization of tensile properties in FSW of AA 5052 to AISI 304 dissimilar joints", Transactions of the Indian Institute of Metals, 69, pp. 891–900, (2016), https://doi.org/10.1007/s12666-015-0572-2.**
7. **Yaduwanshi D., Bag S. , "On the effect of tool offset in hybrid-FSW of copper-aluminium alloy", Materials and Manufacturing Processes, 33(3), pp. 277–287, (2018), DOI: 10.1080/10426914.2017.1279309.**
8. **Liang Z., Chen K., Wang X., Yao J., Yang Q., Zhang L., Shan A., "Effect of tool offset and tool rotational speed on enhancing mechanical property of Al/Mg**

dissimilar FSW joints",Metallurgical and Materials Transactions A, 44, pp. 3721–3731, (2013), https://doi.org/10.1007/s11661-013-1700-4.
9. Ghaffarpour M, Aziz A, Hejazi T. H., "Optimization of friction stir welding parameters using multiple response surface methodology", Proceedings of the Institution of Mechanical Engineers, Part L: Journal of Materials: Design and Applications, 231(7), pp. 571-583 (2017), doi:10.1177/1464420715602139.
10. Essa A. S., Ahmed M. Z., Mohamed. Y. A., El-Nikhaily A. E., "An analytical model for the heat generation in friction stir welding", Modelling and Simulation in Materials Science and Engineering, 12(1), pp. 234-240, (2003), DOI 10.1088/0965-0393/12/1/013.
11. Su H., Wu C. S., Pittner A., Rethmeier M.," Simultaneous measurement of tool torque, traverse force and axial force in friction stir welding", Journal of Manufacturing Processes, 15(4), pp. 495-500, (2013), https://doi.org/10.1016/j. jmapro. 2013.09.001.
12. Sabry I., El-Kassas A. M., "An appraisal of characteristic mechanical properties and microstructure of friction", Journal of Mechanical Engineering and Sciences, 13(4), pp. 5804-5817, (2019), DOI: https://doi.org/10.15282/jmes. 13.4. 2019.07.0463.
13. Sabry I., El-Kassas A. M., Mourad A-H. I. , Thekkuden D. T. and Qudeiri J. A. , "Friction Stir Welding of T-Joints: Experimental and Statistical Analysis. Journal of Manufacturing and Materials Processing, 3(38), pp. 1-23, (2019), DOI: 10.3390/ jmmp3020038.
14. Sabry I., Mourad A-H. I., Thekkuden D. T.,"Comparison of Mechanical Characteristics of Conventional and Underwater Friction Stir Welding of AA 6063 Pipe Joints", International Review of Mechanical Engineering, 14(1), pp. 64-53, (2020), DOI: 10.15866/ireme.v14i1.17483.
15. Sabry I., Mourad A-H., "Optimization of metal inert gas welded aluminium 6061 pipe parameters using analysis of variance and grey relational analysis", SN Applied Sciences, 2(175), (2020), https://doi.org/10.1007/s42452-020-1943-9.
16. Yuvaraj K. P., Jose D. M., Sivasankaran R., Kaushik N., Karuppasamy R., Shanthi C., "Mechanical behaviour of friction stir welded AA7075-T651 and AA6063-T6 joints - an experimental study", Materials Today: Proceedings,, 68(6), pp. 2653-2657, (2022), https://doi.org/10.1016/j.matpr.2022.09.561.
17. Shah L. H., Guo S., Walbridge S., Gerlich A., " Effect of tool eccentricity on the properties of friction stir welded AA6061 aluminum alloys", Manufacturing Letters, 15 (A), pp. 14-17, (2018), https://doi.org/10.1016/j.mfglet.2017.12.019.
18. Aliha M. R. M., Shahheidari M., Bisadi M., Akbari M., Hossain S., "Mechanical and metallurgical properties of dissimilar AA6061-T6 and AA7277-T6 joint made by FSW technique", The International Journal of Advanced Manufacturing Technolog (86), pp. 2551–2565, (2016), DOI: 10.1007/s00170-016-8341-x.
19. Shalin M., Hiten M.,"Experimental Analysis on Effect of Tool Transverse Feed, Tool Rotational Speed And Tool Pin Profile Type on Weld Tensile Strength of Friction Stir Welded Joint of AA 6061", Materials Today: Proceedings, 5(1), pp. 487-493, (2018), https://doi.org/10.1016/j. matpr. 2017.11.109.
20. Amatullah M., Jan M., Farooq M., Zargar A. S., Maqbool A., Khan N. Z., "Effect of tool rotational speed on the friction stir welded aluminum alloys: A

review,“ Materials Today: Proceedings,, 62 (1), pp. 245-250, (2022), https://doi.org/ 10.1016/j.matpr.2022.03.220.
21. Khan N. Z., Siddiquee A. N., Khan Z. A, Shihab S. K.,“Investigations on tunneling and kissing bond defects in FSW joints for dissimilar aluminum alloys”, Journal of Alloys and Compounds, 648, pp. 360-367, (2015), https://doi.org/ 10.1016/j.jallcom.2015.06.246.
22. Sevvel P., Jaiganesh V., “Effects of axial force on the mechanical properties of AZ80A Mg alloy during friction stir welding,“ Materials Today: Proceedings,, 4(2), pp. 1312-1320, (2017), https://doi.org/10.1016/j.matpr.2017.01.152.
23. Sahu P. K., Pal S. K., Jain R., “ Influence of plate position, tool offset and tool rotational speed on mechanical properties and microstructures of dissimilar Al/Cu friction stir welding joints”, Journal of Materials Processing Technology(235), pp. 55-67, (2016), https://doi.org/10.1016/j. jmatprotec. 2016.04.014.
24. Srinivasan R., Ramesh A., Athithanambi A., “ Effect of Axial Force on Microstructure and Mechanical Properties of Friction Stir Welded Squeeze Cast A413 Aluminium Alloy”, Materials Today: Proceedings, 5(5), pp. 13486-13494, (2018). https://doi.org/10.1016/j.matpr.2018.02.344.
25. Mishra R. S., Ma Z. Y., “Friction stir welding and processing”, Materials Science and Engineering: R: Reports, 50 (1-2), (2005), https://doi.org/10.1016/j. mser.2005.07.001.
26. Ramachandran K. K., Murugan N., Shashi K. S., “Friction Stir Welding of Aluminum Alloy AA5052 and HSLA Steel: Mechanical and microstructural characterization of dissimilar friction stir welded butt joints”, Welding Journal, 49 (4), pp. 291-300, (2015).
27. sabry I., “Experimental and Statistical Analysis of Possibility Sources - Rotation Speed, Clamping Torque and Clamping Pith for Quality Assessment in Friction Stir Welding,“ Management and Production Engineering Review, 12(3), pp. 84–96, (2021), DOI: 10.24425/mper.2021.138533.
28. Verma S., Garg D., Misra J. P., Batra U., “ Multi-objective optimum design for FS welded 7039 aluminium alloy considering weld quality issues,“ Materials Today Communications,26(102010), (2021), https://doi.org/ 10.1016/j. mtcomm.2021. 102010.
29. Lakshminarayanan A. K., Balasubramanian V., “ Comparison of RSM with ANFIS in predicting tensile strength of dissimilar friction stir welded AA2024 - AA5083 aluminium alloys”, Procedia Manufacturing, 37, pp. 555-562, (2019), https://doi.org/10.1016/j.promfg.2019.12.088.